Colloids and Surfaces A 529 (2017) 531–540

Contents lists available at ScienceDirect

Colloids and Surfaces A

journal homepage: www.elsevier.com/locate/colsurfa

Adsorption of red azo dyes on multi-walled carbon nanotubes and activated carbon: A thermodynamic study

Guilherme Max Dias Ferreira[a,b], Gabriel Max Dias Ferreira[a,d], Maria C. Hespanhol[a], Jaqueline de Paula Rezende[c], Ana Clarissa dos Santos Pires[c], Leandro Vinícius Alves Gurgel[d], Luis Henrique Mendes da Silva[a,*]

[a] Grupo de Química Verde Coloidal e Macromolecular, Departamento de Química, Universidade Federal de Viçosa (UFV), Av. P. H. Rolfs s/n, 36570900, Viçosa, MG, Brazil
[b] Departamento de Química, Universidade Federal de Lavras (UFLA), Campus Universitário, CP 3037, 37200000, Lavras, MG, Brazil
[c] Departamento de Tecnologia de Alimentos, Universidade Federal de Viçosa, Av. P. H. Rolfs s/n, 36570900, Viçosa, MG, Brazil
[d] Grupo de Físico-Química Orgânica, Departamento de Química, Universidade Federal de Ouro Preto (UFOP), Campus Universitário Morro do Cruzeiro, s/n°, Bauxita, 35400-000 Ouro Preto, MG, Brazil

HIGHLIGHTS

- Ponceau 4R, Congo Red and Allura Red dyes were adsorbed on MWCNT and AC.
- Adsorption of the dyes was enthalpically driven.
- Dyes preferentially interacted with the most hydrophilic sites on the adsorbents.
- Dye charge density and the adsorbent structure determined the dye adsorbed amount.

GRAPHICAL ABSTRACT

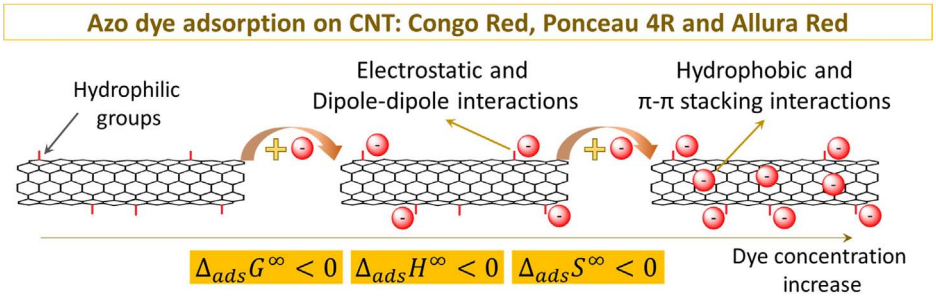

ARTICLE INFO

Keywords:
Adsorption
Azo dyes
Carbon nanotubes
Activated carbons
Calorimetry
Thermodynamics

ABSTRACT

Carbonaceous materials have been extensively studied as highly efficient adsorbents for the removal of dyes from wastewater. However, investigations of thermodynamic aspects of the interactions between these materials and dyes remain scarce. This paper describes the thermodynamics of the interactions between the Ponceau 4R (PR), Congo Red (CR), and Allura Red (AR) dyes and multi-walled carbon nanotubes (MWCNTs). The interactions between the dyes and activated carbon (AC) were also evaluated for comparison. The investigation used a combination of adsorption isotherms and isothermal titration nanocalorimetry (ITC) measurements, and a thermodynamic approach provided full characterization of the adsorption process. For both MWCNT and AC, the amount of adsorbed dye (Γ_D) increased in the order Γ_D (PR) < Γ_D (AR) < Γ_D (CR), and the adsorption capacity normalized by the adsorbent specific area was up to 5.6 times higher for MWCNT. The maximum amount adsorbed ($\Gamma_{D,max}$) reached values of up to 2.00 μmol m^{-2} for CR adsorption on MWCNT. For both adsorbents, the process of dye adsorption was enthalpically driven and entropically unfavorable. All the thermodynamic parameters depended on the surface coverage and the structures of both dye and adsorbent. The adsorption enthalpy change ($\Delta_{ads}H$) and entropy change ($T\Delta_{ads}S^{ref}$) values were higher than −137.0 kJ mol^{-1} and −114.2 kJ mol^{-1}, respectively. In addition to the structural differences between MWCNT and AC, the ITC data

* Corresponding author.
E-mail address: luhen@ufv.br (L.H.M. da Silva).

http://dx.doi.org/10.1016/j.colsurfa.2017.06.021
Received 1 April 2017; Received in revised form 2 June 2017; Accepted 9 June 2017
Available online 15 June 2017
0927-7757/

suggested that the adsorption sites are heterogeneous and that the dyes preferentially adsorb on the more hydrophilic sites on the adsorbent surfaces.

1. Introduction

Most of the synthetic dyes used to give color to several products in textile, leather, paper, and plastic industries, can accumulate in the environment and have high toxicity to human health [1,2]. Thus, the disposal of dyes into water bodies is a serious environmental problem, making the removal of these compounds from wastewater a prominent issue [3,4]. Adsorption is an attractive method for treating dye polluted water. Despite the several types of adsorbents available for this purpose (e.g. layered double hydroxides [5], biomass adsorbents [6], and polymers [7]), carbonaceous materials have attracted great attention due to their high efficiency to adsorb dyes [8–11]. However, most studies investigating dye adsorption on carbonaceous materials, as activated carbons and carbon nanotubes, have focused on determining the adsorption capacities of these materials and/or on the kinetics aspects of the adsorption processes. Thermodynamic aspects, which are very important for fundamental understanding of those adsorptive processes, have not been described in detail, making studies on this research field necessary.

Historically, activated carbon (AC) is the most widely used adsorbent for removing dyes from aqueous solutions [11–15]. AC contains carbons with varying degrees of saturation and oxidation state, and has a high specific surface area (500–2000 $m^2 g^{-1}$) [4]. Its surface has many micropores of different sizes, which are available for dye adsorption, as well as oxygen-containing functional groups that can be chemically modified [16,17]. ACs for dye adsorption can be obtained from various activation methods [11] and from different sources, such as agricultural wastes [18], and bamboo [19]; but economic disadvantages of obtaining those adsorbents should still be overcome [4].

In the last two decades, carbon nanotubes (CNTs) have emerged as a new adsorbent for removing dyes from wastewater [20–23]. Carbon nanotubes, including single-walled carbon nanotubes (SWCNTs) and multi-walled carbon nanotubes (MWCNTs), are cylindrical nanostructures composed essentially of carbon atoms in sp^2 hybridization, which are arranged in a hexagonal lattice with a large specific surface area (100–1000 $m^2 g^{-1}$) [24]. Adsorption of dyes on CNT depends on the physical properties of the nanomaterial [25] and on the adsorbed dye structure [26]. To improve the dye removal efficiency of those adsorbents in practical applications, chemical modification of CNT surface [27–29] and preparation of CNT-based composites [30–32] have been proposed.

Recent studies comparing the adsorption of dyes by different carbonaceous materials [8,27,33,34] showed that the adsorption capacity of CNT can exceed that of AC. However, the application of CNT as adsorbent in environmental remediation applications is still uncertain because of its probable toxicity [35], although the cytotoxic nature of CNT itself can play an important role in the microbial sorption efficiency for treating drinking water [36].

Thermodynamic comprehension of adsorption of dyes on carbonaceous materials could provide important knowledge to develop new cost effective, higher efficient, and environmental friendly carbon-based adsorbents. However, thermodynamic aspects that determine the differences among the behaviors of dye adsorption on CNT and AC have still been poorly investigated. Additionally, most studies have been restricted to obtaining adsorption enthalpies using the van't Hoff approach [9,21,22,34,37], with adsorption constants being obtained from isotherm models describing the system under investigation. In this context, calorimetric measurements arise as a powerful tool to determine adsorption enthalpies.

Calorimetric measurements have been successfully applied to examine the adsorption of both complex biomolecules, such as proteins [38,39], and simple solutes [40–43], including dyes on MWCNT [44]. A comparative study on adsorption of different dyes on AC and CNT surface using calorimetric studies can provide important information about the dye adsorption mechanisms on the surfaces of carbonaceous materials.

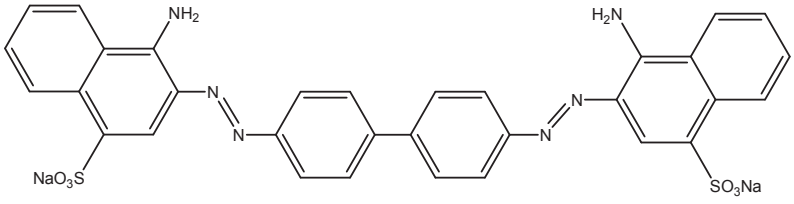

(a)

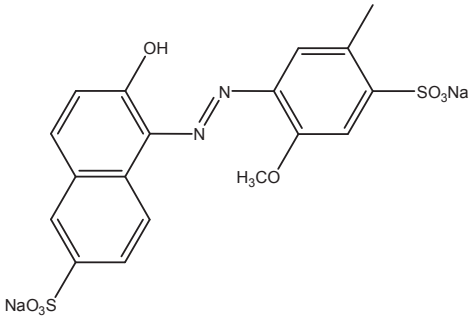

(b)

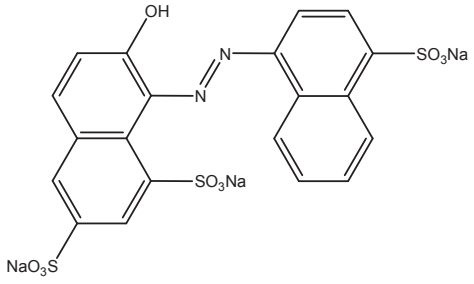

(c)

Fig. 1. Chemical structures of the dyes (a) Congo Red, (b) Allura Red, and (c) Ponceau 4R.

Here, we investigated the thermodynamics of the adsorption of Ponceau 4R (PR), Congo Red (CR), and Allura Red (AR) azo dyes (Fig. 1) on the surfaces of MWCNT and AC in aqueous solutions. Adsorption molar enthalpy changes ($\Delta_{ads}H$) associated with the dye-adsorbent interactions were determined by isothermal titration nanocalorimetry (ITC) as a function of the surface coverage of the adsorbents. Thermodynamic parameters for adsorption at infinite dilution ($\Delta_{ads}H^{\infty}$, $\Delta_{ads}S^{\infty}$, and $\Delta_{ads}G^{\infty}$) were also determined.

2. Experimental

2.1. Chemicals

The multi-walled carbon nanotubes (C_{TUBE} 100 MWCNT) used in this study were obtained from CNT Co. Ltd. (Korea). Activated carbon was purchased from Sigma-Aldrich Chemicals (USA). The dyes Allura Red (E129) (84%, 496.24 g mol^{-1}) and Ponceau Red (E124) (92%, 604.42 g mol^{-1}) were supplied by Gemacom (Brazil). Congo Red (99%, 696.66 g mol^{-1}) was purchased from Merck (Germany). Analytical grade hydrochloric acid and sodium hydroxide, supplied by Vetec (Brazil), were utilized for pH adjustment of the aqueous solutions. All chemicals were used as received, without further purification. Deionized water (Milli-Q) was used to prepare all solutions.

2.2. Characterization of the adsorbents

The specific surface areas of the adsorbents were determined using the Brunauer-Emmett-Teller (BET) equation [45], with values of 188.0 and 868.8 $m^2\ g^{-1}$ obtained for MWCNT and AC, respectively. The points of zero charge (pH_{PZC}) for AC and MWCNT were determined by the solid addition method [46], where 20.0 mg portions of adsorbent were transferred to flasks containing 20.0 mL of 0.01 mol L^{-1} NaCl aqueous solution. The initial pH (pH_i) of the solution was previously adjusted to values between 1.0 and 11.0 by adding either 0.10 mol L^{-1} HCl or 0.10 mol L^{-1} NaOH. The systems obtained were stirred and the final pH values (pH_f) of the solutions were measured after 30 h. For each system, the difference between the initial and final pH values ($\Delta pH = pH_i - pH_f$) was calculated and plotted againstpH_i. The pH_{PZC} was obtained by determining the intercept of the ΔpH versus pH_i curve with the abscissa.

2.3. Adsorption isotherms

Adsorption isotherms were obtained using 10.0 mg of adsorbent (AC or MWCNT) dispersed in 10.0 mL of the dye solution in 30.0 mL cylindrical glass flasks. The dye concentration in the solutions ranged from 0 to 900.0 mg L^{-1}. The systems were manually stirred for 15 min and then placed in a temperature-controlled bath for 24 h, where they remained at rest. This time was enough for the systems reaching the thermodynamic equilibrium. Subsequently, the supernatant was collected for analysis of the dye concentration. When activated carbon was used as the adsorbent, the systems were centrifuged at 10,000 rpm for 40 min in a Heraeus Megafuge 11R centrifuge (Thermo Scientific) in order to separate the adsorbent from the aqueous solution.

The equilibrium concentrations of the dyes in the supernatants were determined by spectrophotometry, using a digital double-beam spectrometer (UV-2550, Shimadzu). Absorbance measurements were made at 332, 498, and 314 nm for PR, CR, and AR, respectively. The amount of dye adsorbed (Γ_D), in μmol m^{-2}, was calculated using the following equation:

$$\Gamma_D = \frac{(C_0 - C_e)\cdot V}{m\cdot A} \tag{1}$$

where C_0 and C_e are the initial and equilibrium concentrations, respectively, of dye in the supernatant (in μmol L^{-1}), m is the mass of the adsorbent (in kg), V is the volume of the supernatant (in L), and A is the BET specific surface area of the adsorbent (in $m^2\ kg^{-1}$).

The effect of the initial pH on the amount of dye adsorbed was evaluated in the pH range between 1.0 and 12.0 for the PR and AR dyes, and between 5.0 and 12.0 for CR. The CR dye was unstable and/or insoluble at pH values below 4.0, at the concentrations evaluated. For these experiments, the dye concentrations were fixed at 200 mg L^{-1} for PR and AR, using both adsorbents. For CR, the concentrations evaluated were 100 and 200 mg L^{-1} using AC and MWCNT, respectively.

All the measurements were carried out at 298.15 K. The experiments were performed in duplicate and the Γ_D values were the averages of the two determinations. The relative standard deviations were lower than 5%.

2.4. Adsorption thermodynamic parameters

Thermodynamic analysis of dye adsorption was conducted by determining the adsorption Gibbs free energy change ($\Delta_{ads}G^{ref}$), the adsorption enthalpy change ($\Delta_{ads}H$), and the adsorption entropy change ($\Delta_{ads}S^{ref}$). The superscript "*ref*" was used to designate the reference state.

2.4.1. Adsorption Gibbs free energy change

To obtain $\Delta_{ads}G^{ref}$, a thermodynamic approach was used in which the dye adsorption process was considered to involve partitioning of the dye between the liquid phase and the liquid-solid interface. The equilibrium thermodynamic constant (K_{ads}) for the dye adsorption is given by:

$$K_{ads} = \left(\frac{\gamma_D^S \Gamma_D}{\gamma_D^{sol} C_e}\right) \tag{2}$$

where γ_D^S and γ_D^{sol} are the activity coefficients of the dye in the adsorbent surface and in the solution, respectively. The molar Gibbs free energy change of adsorption for the transfer of the dye between two reference states, $\Delta_{ads}G^{ref}$, can be obtained from the K_{ads} value, according to Eq. (3):

$$\Delta_{ads}G^{ref} = \mu_D^{ref,S} - \mu_D^{ref,sol} = -RTlnK_{ads} \tag{3}$$

where $\mu_D^{ref,S}$ and $\mu_D^{ref,sol}$ are the chemical potentials of the dye at the adsorbent surface and in the solution, respectively, in the reference state; T is the absolute temperature of the system, and R is the universal gas constant.

Considering that at infinite dilution the dye activity coefficient is equal to unity, the hypothetical reference state of the dye can be defined as that where the dye activity coefficient tends to unity when the dye concentration approaches unity. Eq. (2) can then be used to determine K_{ads} at infinite dilution, according to Eq. (4):

$$K_{ads} = \lim_{c_e \to 0} \frac{\Gamma_D}{C_e} \tag{4}$$

where Γ_D is given in mg g^{-1} and C_e is in mg L^{-1}. Therefore, K_{ads} values can be easily obtained from the isotherm data, enabling determination of $\Delta_{ads}G^{\infty}$, where the superscript ∞ refers to the reference state at infinite dilution. The $\Delta_{ads}G^{\infty}$ parameter expresses the change in the Gibbs free energy of the system when one mol of solute moves from the liquid solution to the adsorbent surface in the standard state under infinite dilution conditions (i.e., when there are no dye-dye interactions at the adsorbent surface or in the solution).

Blaschke et al. [47] proposed a thermodynamic approach that allows $\Delta_{ads}G^{ref}$ to be obtained for different reference states, where a new reference state was established at a defined (but arbitrary) point on the adsorption isotherm, with concentration C_e^{ref}. The equilibrium constant (K_{ads}^*) and $\Delta_{ads}G^{ref}$ can then be obtained using Eqs. 5 and 6:

$$K_{ads}^* = \lim_{C_e \to C_e^{ref}} \left(\frac{\Gamma_D}{C_e}\right) \tag{5}$$

$$\Delta_{ads}G^{ref} = -RT\ln K^{*}_{ads} \quad (6)$$

A detailed discussion of this procedure is provided by Blaschke et al. [47]. Using this approach, $\Delta_{ads}G^{ref}$ can be obtained for any solute concentration.

2.4.2. Adsorption molar enthalpy change

The adsorption molar enthalpy change ($\Delta_{ads}H$) associated with dye-adsorbent interaction was determined using a TAM III Isothermal Titration Nanocalorimeter (TA Instruments) controlled by dedicated TAM Assistant™ software. This calorimeter is equipped with two reaction cells (sample and reference cells) with volumes of 4.00 mL. The calorimetric procedure was based on a previous report [48] and the titrations were carried out by stepwise 15 μL injections of a concentrated aqueous dye solution into the sample cell containing 4.00 mg of adsorbent (MWCNT or AC) and 2.70 mL of deionized water. The injections were made using a Hamilton syringe (500 μL) controlled by a 3810 syringe pump (TA Instruments). The time interval between two consecutive injections was 60 min, and a stirrer helix operated at 180 rpm was used in the sample cell to ensure homogenization during the titration. Blank experiments were also performed, with (i) addition of dye solution in deionized water in the absence of the adsorbents, and (ii) addition of deionized water to 4.00 mg of each adsorbent plus deionized water. The latter procedure revealed negligible thermal effects. For all experiments, the reference cell was filled with deionized water and the measurements were performed at a temperature of 25.0000 ± 0.0001 °C. Each experiment was carried out in duplicate.

The adsorption enthalpy change at different Γ_D values (for the *i-th* injection of the dye solution in the sample cell), $\Delta_{ads}H$, was determined using Eq. (7):

$$\Delta_{ads}H = \frac{q_{i,ads} - q_{i,dil}}{n_i} \quad (7)$$

where $q_{i,ads}$ and $q_{i,dil}$ are the heat absorbed or released in the sample cell, with and without adsorbent, respectively, for the *i-th* injection of the aqueous dye solution, and n_i is the amount of dye that adsorbs on the MWCNT (or AC) surface for the same injection. The n_i values were determined directly from the adsorption isotherms. The relative standard deviations for $\Delta_{ads}H$ were lower than 10%.

The integral adsorption enthalpy change ($\Delta_{ads}H_{integral}$) was also determined, using the following equation:

$$\Delta_{ads}H_{integral} = \frac{\sum_i (q_{i,ads} - q_{i,dil})}{\sum_i n_i} \quad (8)$$

where $q_{i,ads}$, $q_{i,dil}$, and n_i have the same meanings as in Eq. (7). The $\Delta_{ads}H_{integral}$ parameter contains the energetic contributions of all occupied adsorption sites to the enthalpy change of the adsorption process (for each surface coverage). The relative standard deviations for $\Delta_{ads}H_{integral}$ were lower than 6%.

2.4.3. Adsorption entropy change

Adsorption molar entropy changes for each defined reference state ($\Delta_{ads}S^{ref}$) were calculated from the classic thermodynamic relationship:

$$\Delta_{ads}G^{ref} = \Delta_{ads}H - T\Delta_{ads}S^{ref} \quad (9)$$

3. Results and Discussion

3.1. Adsorption isotherms

The adsorption of a solute on a surface depends on a delicate balance between the interactions that the solute establishes with the components in the solution and at the interface. Some aspects of these interactions can be understood by evaluating the equilibrium data presented by an adsorption isotherm. Fig. 2 shows the adsorption isotherms of the red dyes on the MWCNT surface, at 25 °C and pH_i = 6.0.

For all dyes, the Γ_D values increased as the C_e values increased, until reaching a maximum value ($\Gamma_{D,max}$) that indicated saturation of the MWCNT surface. However, for each dye equilibrium concentration, the Γ_D values depended strongly on the structure of the dye molecule, increasing in the order Γ_D (PR) < Γ_D (AR) < Γ_D (CR). The highest observed Γ_D values ranged from 0.598 ± 0.026 μmol m^{-2} (67.9 ± 2.9 mg g^{-1}) for PR to 1.96 ± 0.01 μmol m^{-2} (256 ± 2 mg g^{-1}) for CR, and were on the same order of magnitude as the values obtained for other dyes on the MWCNT surface [8].

Despite the larger molecular size of CR (Fig. 1), this dye showed a $\Gamma_{D,max}$ value 3.3 times higher than obtained for PR. The CR dye molecule has more benzene rings in its structure (six, three, and four benzene rings are present in the structures of CR, AR and PR, respectively), making it the most hydrophobic dye, with the greatest capacity to bind to the aromatic structure of MWCNT by π-π stacking interactions. The results therefore suggest important contributions of π-π stacking and hydrophobic interactions in azo dye adsorption on the MWCNT surface.

Hydrophobic and π-π stacking interactions have been proposed previously as the main forces responsible for the adsorption of organic molecules on CNTs [49]. However, other important contributions to this process that have been proposed are electrostatic interactions and the molecular conformation of the adsorbed molecules [17,26]. The latter effect provides an explanation for the fact that the PR dye, which has a greater number of benzene rings than AR, presented slightly lower Γ_D values. The π-π interactions are favored when the dye approaches the MWCNT in a face-to-face conformation, which is more likely for AR than PR because the steric hindrance caused by the extra sulfonate group in the PR structure prevents coplanarity of the four aromatic rings of PR. According to Almeida et al. [50], the two naphthol rings in the PR molecule are found up to 12.8° out-of-plane relative to one another.

A better understanding of the adsorption of the red dyes on the MWCNT surface can be obtained by examining the differences between the adsorption processes of the dyes on the surfaces of different carbonaceous materials. Activated carbon (AC) was used for this purpose, because its surface possesses a large quantity of functional groups containing oxygen atoms, making it less hydrophobic than MWCNT. In addition, AC contains carbon atoms with varying degrees of saturation and different oxidation states, and has a low content of graphitized

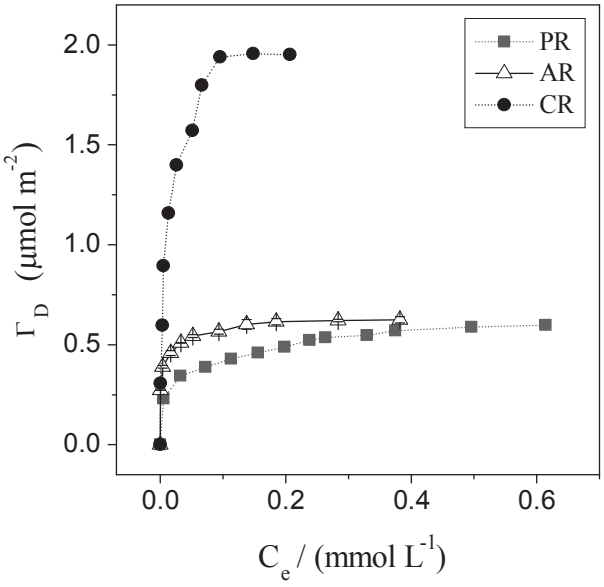

Fig. 2. Adsorption isotherms of red dyes on the MWCNT surface, at 25.0 °C and pH_i = 6.0.

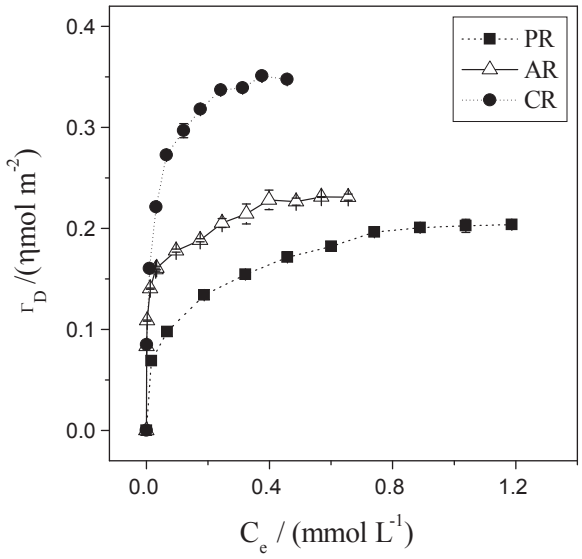

Fig. 3. Adsorption isotherms of red dyes on the AC surface, at 25.0 °C and pH_i = 6.0.

structures [17]. The adsorption isotherms of the CR, PR, and AR dyes on the AC surface, at 25.0 °C and pH_i = 6.0, are presented in Fig. 3.

Considering the effect of the dye structure on the amount adsorbed, the Γ_D values for AC also followed the order Γ_D (PR) < Γ_D (AR) < Γ_D (CR), showing that the interactions that governed the adsorption of the dyes on this adsorbent were similar to those that influenced adsorption on the MWCNT surface. However, the Γ_D values were higher for MWCNT than for AC, at all equilibrium concentrations, and the $\Gamma_{D,max}$ values were at least 2.7 times greater when MWCNT was used as the adsorbent. These results suggest that the hydrophobic and π-π stacking interactions between the dye and the adsorbent are more favorable for MWCNT than AC.

In an additional analysis, the $\Gamma_{D,max}$ (AR)/$\Gamma_{D,max}$ (PR) and $\Gamma_{D,max}$ (CR)/$\Gamma_{D,max}$ (AR) ratios were calculated for MWCNT and AC, using the experimental data. The $\Gamma_{D,max}$ (AR)/$\Gamma_{D,max}$ (PR) ratio remained almost constant when MWCNT was replaced by AC, with values of 1.04 and 1.13, respectively. The $\Gamma_{D,max}$ (CR)/$\Gamma_{D,max}$ (AR) ratio decreased by half, from 3.14 for MWCNT to 1.52 for AC. These results suggest that the AC has a high percentage of the surface area unavailable for dye adsorption, notably in the case of CR, which has a larger molecular size than the other dyes studied.

The Γ_D value depends on the surface area available for dye adsorption. AC is a porous material with a large quantity of narrow micropores that are inaccessible for various chemicals including dyes [17,51]. On the other hand, the pores of MWCNT are formed by the entanglement of individual tubes that interact due to van der Waals forces. These pores have dimensions of mesopores or higher, so they are more accessible to the adsorbate, compared with the pores of AC [34,52]. Hence, the $\Gamma_{D,max}$ (CR)/$\Gamma_{D,max}$ (AR) ratio decreased when MWCNT was replaced with AC, because some pores of AC could not be accessed by CR molecules, due to their larger size relative to AR. This pore size effect did not affect the $\Gamma_{D,max}$ (AR)/$\Gamma_{D,max}$ (PR) ratio, probably because the AR and PR molecules are similar in size and could therefore access the same numbers of sites on the adsorbents. When the Γ_D values were expressed in mmol kg^{-1}, the adsorption capacities for PR and AR were higher for AC, because the specific surface area of this adsorbent was higher ($A_{AC} \approx 4.6A_{MWCNT}$). However, for CR, the adsorption capacity remained higher for MWCNT, showing that the effect of pore size on the adsorption was more pronounced for this dye.

The adsorption capacities of AC and MWCNT surfaces have been compared for other dye molecules. Machado et al. [34] evaluated the adsorption of Reactive Red M-2BE on MWCNT and AC and reported maximum dye uptakes of 335.7 mg g^{-1} (1.9 μmol m^{-2}) and 260.7 mg g^{-1} (0.4 μmol m^{-2}), respectively. Li et al. [27] studied the adsorption capacities of CNT and AC for Methylene Blue and found $\Gamma_{D,max}$ values of 1.23 and 0.16 mg m^{-2}, respectively. In both studies, the authors proposed that the difference between the adsorption capacities was due to the larger pore diameter of the CNT when compared with AC.

Although the pore diameter of the adsorbent is important in terms of adsorption capacity, here we are more interested in the thermodynamic aspects of the binding of the dyes on the surfaces of the adsorbents. In order to understand these aspects, it is important to evaluate the contribution of electrostatic interactions in the adsorption process.

3.2. Influence of pH on dye adsorption

The pH of the system can have a major influence on the adsorptive uptake of a solute on a surface. This is because the hydrogen ion concentration can govern the net charge of the adsorbent and the degree of ionization/dissociation of the solute, which determine the electrostatic

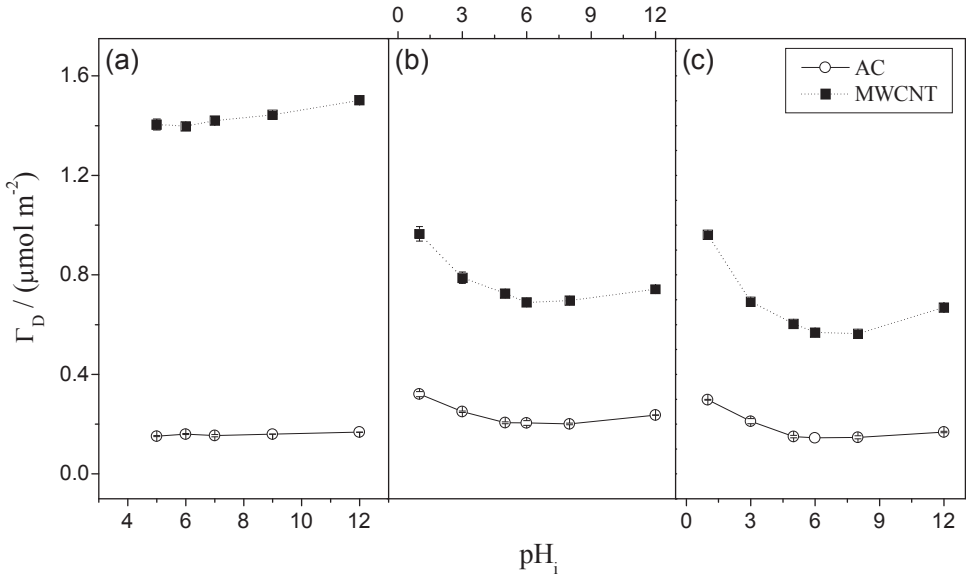

Fig. 4. Effect of initial pH on the adsorption of the red dyes by MWCNT and AC, at 25.0 °C: (a) CR, (b) AR, and (c) PR. The dye concentrations were fixed at 200 mg L^{-1} for PR and AR using both adsorbents and at 100 and 200 mg L^{-1} for CR using AC and MWCNT, respectively.

interaction between the dye and the adsorbent. Hence, evaluation of the effect of pH on the adsorption of the red dyes can provide valuable information about the importance of electrostatic interactions in this process. Fig. 4 shows the effect of the initial pH of the system on the amount of adsorbed dye for the MWCNT and AC surfaces.

The profiles of the Γ_D versus pH_i curves were slightly affected by the structures of the dye and adsorbent, suggesting that the electrostatic forces acting in the adsorption process were equally affected by pH for all the systems evaluated. In the case of CR, when pH_i was increased from 5.0 to 12.0, the Γ_D values increased slightly from 0.15 to 0.17 μmol m^{-2} for AC and from 1.40 to 1.50 μmol m^{-2} for MWCNT. For AR and PR, the Γ_D values decreased when pH_i was increased from 1.0 to 6.0, followed by a slight increase when the pH_i was raised to 12.0.

In the pH_i range evaluated, the red dyes are always negatively charged, due to the presence of sulfonate groups (sulfonic acid has pK_a near 0), while the charge on AC and MWCNT surfaces depends on the pH. At pH lower than the point of zero charge (pH_{PZC}), the adsorbents have positive surface net charge, while at pH higher than pH_{PZC} they have negative net charge. The pH_{PZC} of the MWCNT and AC adsorbents were estimated to be 7.5 and 8.6, respectively (Fig. S1).

For AR and PR, at pH_i 1.0 there were electrostatic attractions between the positively charged surfaces of the adsorbents (pH < pH_{PZC}) and the anionic dyes. As the pH of the system increased up to the pH_{PZC}, the positive surface charge on the adsorbent was reduced. Therefore, the electrostatic attraction between the dyes and the adsorbents became weaker and the Γ_D values decreased, reaching the lowest values at around pH_{PZC}. However, the Γ_D values remained high, confirming that non-electrostatic interactions also participated in the adsorption process.

At pH_i 12.0 (pH > pH_{PZC}), the negative surface charge density on the MWCNT and AC increased, intensifying the repulsive electrostatic interactions between the adsorbents and the anionic dyes. A decrease in the Γ_D values would therefore be expected at this pH. However, this was not observed and there was a slight increase in the Γ_D values, suggesting electrostatic shielding between the dyes and the adsorbent surfaces. This shielding resulted from the increase in the ionic strength caused by Na^+ ions from the NaOH used to adjust the pH of the solution.

3.3. Adsorption thermodynamic parameters

3.3.1. Adsorption of AR on MWCNT

Until now, we have characterized the dye-adsorbent interaction from a qualitative perspective. However, quantitative information is needed in order to better understand the driving forces governing dye adsorption on the surfaces of carbonaceous materials. Therefore, the thermodynamic parameters ($\Delta_{ads}G^{ref}$, $\Delta_{ads}H^{ref}$, and $\Delta_{ads}S^{ref}$) for dye adsorption on the MWCNT and AC surfaces were determined for different surface coverage of the adsorbents.

Fig. 5 shows plots of $\Delta_{ads}G^{ref}$, $\Delta_{ads}H^{ref}$, and $T\Delta_{ads}S^{ref}$ against Γ_D for AR adsorption on the MWCNT surface, at 25.0 °C and pH_i equal to 6.0. The $\Delta_{ads}X^{ref}$ values for higher Γ_D could not be calculated, because the difference between the calorimetric signals obtained from the dilution of the dye and from the adsorption experiments was equal to the equipment noise, which could be attributed to the small amount of dye that adsorbed on the MWCNT for each injection, when the adsorbent surface was almost saturated.

The $\Delta_{ads}G^{ref}$ values for AR adsorption on MWCNT were always negative, indicating that the dye was concentrated on the MWCNT surface under equilibrium conditions. The $\Delta_{ads}H$ and $T\Delta_{ads}S^{ref}$ values were also negative, within the Γ_D range evaluated, showing that the dye adsorption process was enthalpically driven for the entire range of surface coverage. However, the Γ_D increase resulted in the $\Delta_{ads}H$ and $T\Delta_{ads}S^{ref}$ values becoming less negative, suggesting that the AR-MWCNT interaction occurred at different adsorption sites and/or that the AR molecules began to interact strongly among themselves, on the adsorbent surface and in the bulk solution, as the dye concentration increased.

Analysis of the profile of the $\Delta_{ads}H$ versus Γ_D curve provided information about the interactions that dominated the adsorption process as the surface coverage increased. At Γ_D of 8.69×10^{-2} μmol m^{-2}, corresponding to the first injection in the calorimetric titration experiment, $\Delta_{ads}H$ was -124 kJ mol^{-1}, indicating that hydrogen bonds, electrostatic and dipole-dipole interactions were involved in the adsorption process.

To explain the profile of the plot of $\Delta_{ads}H$ against Γ_D, and the magnitude of the $\Delta_{ads}H$ values (Fig. 5), $\Delta_{ads}H$ was considered to be the sum of terms associated with four independent sub-processes occurring during the dye adsorption. These different contributions are shown in Eq. (10):

$$\Delta_{ads}H = \Delta_{ads}H^{des} + \Delta_{ads}H^{D-S} + \Delta_{ads}H^{D-D,Sur} + \Delta_{ads}H^{D-D,Sol} \quad (10)$$

In Eq. (10), $\Delta_{ads}H^{des}$ is the enthalpy change associated with the desolvation process of the dye and adsorbent, involving (i) the breaking of water-dye and water-adsorbent interactions, (ii) the creation of water-water interactions, and (iii) the change in the solvation shell structure of the adsorbent due to the dye adsorption. This term can be positive or negative, depending on the energetic balance between the interactions formed and disrupted during the process. $\Delta_{ads}H^{D-S}$ is the enthalpy change for the interaction between the dye and the surface adsorption sites, and is always negative. The terms $\Delta_{ads}H^{D-D,Sur}$ and $\Delta_{ads}H^{D-D,Sol}$ are the enthalpy changes resulting from dye-dye interactions on the adsorbent surface and in the solution, respectively. During the adsorption process, the term $\Delta_{ads}H^{D-D,Sur}$ should be positive because it involves the repulsive electrostatic interactions between the negatively charged dye molecules on the adsorbent surface. On the other hand, the sign of the term $\Delta_{ads}H^{D-D,Sol}$ can be positive or negative, and this information can be obtained from the slopes of the ITC dilution curves of the dyes. Our results showed that $\Delta_{ads}H^{D-D,Sol}$ should be positive for AR, becoming less positive for higher concentrations (see Fig. S2 and discussion in supplementary material).

At low Γ_D values, there were few AR molecules in the solution and on the MWCNT surface. For instance, in the first injection during the calorimetric experiment, the AR concentration in the solution in the sample cell was 2.7×10^{-8} mol L^{-1} and the average area available for each adsorbed AR molecule was about 19 nm^2 (for comparison, the CR molecule, which was the longest molecule studied here, has a maximum extension of 2.5 nm [53]). Therefore, the AR-AR interactions in the solution and at the interface were negligible, and the $\Delta_{ads}H^{D-D,Sur}$ and $\Delta_{ads}H^{D-D,Sol}$ terms in Eq. 10 did not contribute to the magnitude of $\Delta_{ads}H$. Hence, the $\Delta_{ads}H$ values were negative because $\Delta_{ads}H^{des} + \Delta_{ads}H^{D-S} < 0$. Whereas $\Delta_{ads}H^{D-S}$ term was always negative, the $\Delta_{ads}H^{des}$ term could be either negative or positive, but

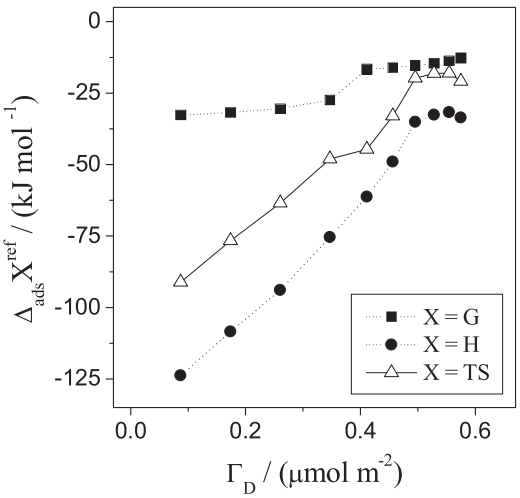

Fig. 5. Adsorption thermodynamic parameters versus Γ_D curves for adsorption of AR on MWCNT, at 25.0 °C and pH_i = 6.0.

$|\Delta_{ads}H^{des}| < |\Delta_{ads}H^{D-S}|$.

When the Γ_D values increased, the dye-dye interaction became important and the $\Delta_{ads}H^{D-D,Sur}$ and $\Delta_{ads}H^{D-D,Sol}$ terms began to contribute to the $\Delta_{ads}H$ values; the higher the dye concentration, the more positive was the $\Delta_{ads}H^{D-D,Sur}$ term, because the electrostatic repulsion increased as a result of the decrease in the distance of interaction between the dye molecules on the surface. On the other hand, an opposite tendency was observed for the $\Delta_{ads}H^{D-D,Sol}$ term, which became less positive as the AR concentration increased (Fig. S2). At the same time, the sites of the adsorbent that interacted more favorably with the dye, releasing a greater amount of heat (these were probably the less hydrophobic interaction sites), became unavailable for dye adsorption, so the dye started to interact with less favorable sites, making the $\Delta_{ads}H^{D-S}$ term less negative. Therefore, the $\Delta_{ads}H$ values became less negative as the surface coverage increased due to the increase in the $\Delta_{ads}H^{D-D,Sur}$ and $\Delta_{ads}H^{D-S}$ values and the decrease in the $\Delta_{ads}H^{D-D,Sol}$ term.

The change in the adsorption entropy can result from two main events: (i) transfer of the dye from the solution to the solid-liquid interface, which decreases the entropy of the system, due mainly to the decrease in the configurational entropy of the dye on the adsorbent surface; and (ii) the release of water molecules from the solvation layer of both solute and adsorbent, which increases the entropy of the system. Hence, the $T\Delta_{ads}S^{ref}$ values were negative because the entropy gain due to the release of water molecules during the process of dehydration of MWCNT and AR did not compensate the loss of entropy due to the decrease in the degree of freedom of the dye. However, the entropy gain due to the release of water molecules from the dehydration process increased when Γ_D increased because the hydrophobic interactions between AR and MWCNT became more important at higher Γ_D values, as suggested from the $\Delta_{ads}H$ calorimetric curves. Consequently, $T\Delta_{ads}S^{ref}$ increased at higher surface coverage.

3.3.2. Effect of the dye structure

To investigate the effect of the dye structure on the adsorption thermodynamic parameters and obtain more information about the mechanism of interaction between MWCNT and the azo dyes, $\Delta_{ads}G^{ref}$, $\Delta_{ads}H$, and $T\Delta_{ads}S^{ref}$ versus Γ_D curves were also obtained for the CR and PR dyes (Fig. 6).

For both CR and PR, the $\Delta_{ads}G^{ref}$ values were also negative, and the dependence of this parameter on Γ_D was similar to that observed for the AR dye. However, the profiles of the $\Delta_{ads}H$ and $T\Delta_{ads}S^{ref}$ versus Γ_D curves were strongly dependent on the dye structure.

For the CR dye (Fig. 6a), the $\Delta_{ads}H$ and $T\Delta_{ads}S^{ref}$ values increased when the Γ_D value changed from 0.11 to 0.24 μmol m^{-2}. They then remained almost constant when the Γ_D values increased up to 0.94 μmol m^{-2}, indicating that the occupied adsorption sites interacted with the dye, releasing equal amounts of energy in this Γ_D range. When Γ_D was greater than 0.94 μmol m^{-2}, the $\Delta_{ads}H$ and $T\Delta_{ads}S^{ref}$ values increased as Γ_D increased up to 1.36 μmol m^{-2}, and then remained constant again.

At Γ_D of 0.11 μmol m^{-2}, there was an important contribution of the hydrophilic sites to CR adsorption, leading to a more exothermic process due to the more negative $\Delta_{ads}H^{D-S}$ values. In the range from 0.24 to 0.94 μmol m^{-2}, the different behavior of the $\Delta_{ads}H$ versus Γ_D curve for CR, compared with the AR dye, was due to the low charge density and high hydrophobicity of this dye, associated with the presence of mainly hydrophobic sites on the MWCNT surface. Because of this, the $\Delta_{ads}H^{D-D,Sur}$ term did not make a large contribution to $\Delta_{ads}H$, while the $\Delta_{ads}H^{D-S}$ term was almost constant. Therefore, the $\Delta_{ads}H$ values showed little variation for this wide range of surface coverage.

As the Γ_D values increased above 0.83 μmol m^{-2}, the $\Delta_{ads}H^{D-D,Sur}$ term became important and the $\Delta_{ads}H$ term increased. Above 1.36 μmol m^{-2}, the CR concentration in the solution became higher than 48.7 μmol L^{-1}, and beyond this concentration an important molecular event contributed to the magnitude of $\Delta_{ads}H$. Fig. S2b shows the ITC dilution curve of CR dye in the concentration range from 0 to 85 μmol L^{-1}. The sigmoid profile of this curve was due to the ability of CR to form dimers [54]. The dimerization process occurs at 48.7 μmol L^{-1} and has an energetic cost of 7.7 kJ mol^{-1} (details are showed in Fig. S2b). Consequently, when Γ_D was equal to 1.36 μmol m^{-2} in the calorimetric cell, the CR dye molecules in the solution formed dimers, and as the adsorption process occurred, the dimers were broken before adsorbing, releasing enthalpic energy that compensated the contribution of $\Delta_{ads}H^{D-D,Sur}$ and made the $\Delta_{ads}H$ values constant again.

Comparison between the thermodynamic parameter versus Γ_D curves for AR and CR also provided valuable information about the mechanisms involved in the adsorption of the dyes on MWCNT (an easier comparison of the curves obtained for AR and CR is provided in Figs. S3 and S4). Results suggested that the higher hydrophilic/hydrophobic balance of AR contributed to more negative $\Delta_{ads}H$ values for this dye than CR (see discussion in supplementary material).

Explanation of the relative magnitudes of the $T\Delta_{ads}S^{ref}$ values for AR and CR requires consideration of the changes of entropy that occurred in the bulk solution and at the interface when the dyes adsorbed. However, this parameter cannot be directly compared in the graph of $T\Delta_{ads}S^{ref}$ versus Γ_D (Fig. S4), because at the same Γ_D value the dye concentrations in the solution were very different. For example, when Γ_D was equal to 0.46 μmol m^{-2}, the C_e value for AR was about 6.5 times higher than for CR. Therefore, when the dyes were transferred from the solution to the adsorbent surface, the contributions of the configurational entropy change to the $T\Delta_{ads}S^{ref}$ value were different for the two dyes and no molecular information could be obtained.

For the PR dye (Fig. 6b), the process of adsorption on MWCNT was also enthalpically driven. However, the profiles of the Δ_{ads}H and

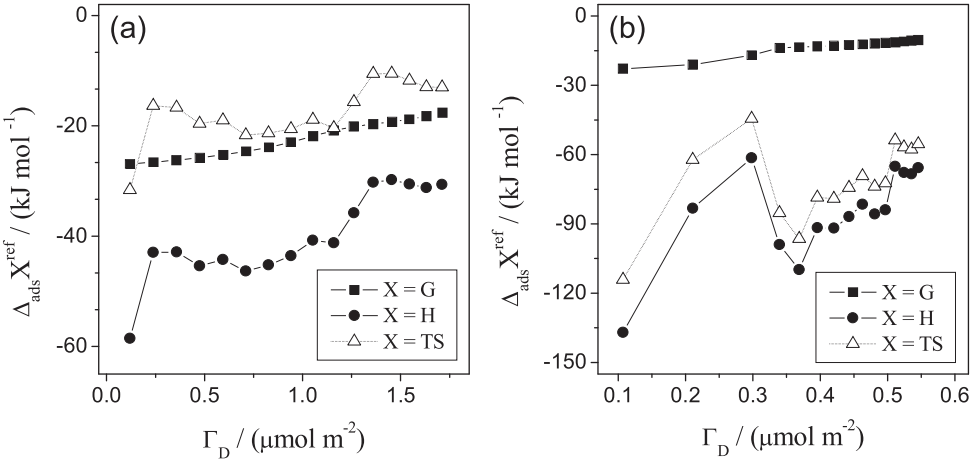

Fig. 6. Adsorption thermodynamic parameters versus Γ_D curves for adsorption of (a) CR and (b) PR on MWCNT, at 25.0 °C and pH_i = 6.0.

$T\Delta_{ads}S^{ref}$ versus Γ_D curves for this dye were very different from those observed for AR and CR. As Γ_D changed from 0.11 to 0.30 μmol m^{-2}, the $\Delta_{ads}H$ and $T\Delta_{ads}S^{ref}$ values became less negative. Subsequently, increase of Γ_D from 0.30 to 0.37 μmol m^{-2} rendered the adsorption process more exothermic and more entropically unfavorable. Finally, above 0.37 μmol m^{-2}, increase of Γ_D led to slight increases of $\Delta_{ads}H$ and $T\Delta_{ads}S^{ref}$. This behavior suggests that different molecular events during the adsorption of PR modulated the enthalpic/entropic balance.

3.3.3. Effect of the adsorbent surface

The effect of the adsorbent surface on the thermodynamics of dye adsorption was evaluated by constructing plots of $\Delta_{ads}G^{ref}$, $\Delta_{ads}H$, and $T\Delta_{ads}S^{ref}$ against Γ_D for AC (Fig. S5). In most cases, the replacement of MWCNT by AC did not alter the curve profiles, except in the case of the CR dye. Fig. 7 presents the curves for CR adsorption on MWCNT and AC. The comparison between the adsorption thermodynamic parameters was limited to the range between 0.12 and 0.28 μmol m^{-2}, because the amounts of CR adsorbed on the MWCNT and AC surfaces were very different.

Although the $\Delta_{ads}G^{ref}$ values became less negative when MWCNT was replaced by AC (Fig. 7a), the dye adsorption process remained enthalpically driven (Fig. 7b). However, two differences in the $\Delta_{ads}H$ versus Γ_D curves should be highlighted: (i) the difference between the magnitudes of the Δ_{ads}H(MWCNT) and Δ_{ads}H(AC) values, and (ii) the absence of a plateau in the curve for CR adsorption by AC. These features were associated with the greater heterogeneity of the sites on the AC surface, compared with those on MWCNT. Additionally, there was strong dye-dye interaction on the AC surface, even at the beginning of the adsorption process (low Γ_D values), as shown by the steep slope of the $\Delta_{ads}H$ versus Γ_D curve. Therefore, the $\Delta_{ads}H^{D-D,Sur}$(AC) value made a substantial contribution to Δ_{ads}H(AC). This second hypothesis can be explained by the inaccessible surface area of AC, with a smaller surface area available for the adsorption of CR molecules.

3.4. Adsorption thermodynamic parameters under infinite dilution conditions

The driving forces responsible for dye adsorption on AC and MWCNT in the absence of dye-dye interaction were investigated by determining the adsorption thermodynamic parameters under infinite dilution conditions. The adsorption Gibbs free energy change for infinite dilution was determined using the equation: $\Delta_{ads}G^{\infty} = -RT\ln K_{ads}$, where K_{ads} was obtained using Eq. (4). The adsorption enthalpy change for infinite dilution ($\Delta_{ads}H^{\infty}$) was obtained from extrapolation of the integral adsorption enthalpy change ($\Delta_{ads}H_{integral}$) versus Γ_D curves for $\Gamma_D \rightarrow 0$ (Fig. S6). Finally, the adsorption molar entropy change at infinite dilution ($\Delta_{ads}S^{\infty}$) was obtained using Eq. (9). Table 1 shows the adsorption thermodynamic parameters at infinite dilution for the systems studied.

The $\Delta_{ads}G^{\infty}$ values were negative for all the systems, indicating that the dye was concentrated on the adsorbent surface at equilibrium under infinite dilution conditions. Under these conditions, the adsorption process was enthalpically driven ($\Delta_{ads}H^{\infty} < 0$) and entropically unfavorable ($T\Delta_{ads}S^{\infty} < 0$), with both $\Delta_{ads}H^{\infty}$ and $T\Delta_{ads}S^{\infty}$ values increasing in the order PR < AR < CR.

Table 1
Thermodynamic parameters under infinite dilution conditions for adsorption of red dyes on AC and MWCNT, at 25.0 °C and pH_i = 6.0.

Dye	$\Delta_{ads}G^{\infty}$ (kJ mol^{-1})		$\Delta_{ads}H^{\infty}$ (kJ mol^{-1})[a]		$T\Delta_{ads}S^{\infty}$ (kJ mol^{-1})	
	MWCNT	AC	MWCNT	AC	MWCNT	AC
CR	−27.24	−29.38	−76.02	−71.63	−48.78	−42.25
AR	−33.31	−28.54	−132.72	−133.64	−99.41	−105.1
PR[b]	−23.89	−22.09	−198.78	−182.32	−174.89	−160.23

[a] Relative standard deviations were lower than 4.0%.
[b] $\Delta_{ads}H^{\infty}$ and $T\Delta_{ads}S^{\infty}$ were not obtained with accuracy for the PR dye due to the low amount of data for the fitted model (Fig. S6).

For both adsorbents, the $\Delta_{ads}G^{\infty}$ values were dependent on the structure of the dye. Despite the small change in $\Delta_{ads}G^{\infty}$ when the dye structure was changed ($\Delta_{ads}G^{\infty}$ changed by a maximum of 9.42 kJ mol^{-1} for MWCNT when AR was replaced by PR), the $\Delta_{ads}H^{\infty}$ and $T\Delta_{ads}S^{\infty}$ values varied over a wide range, with maximum changes of 122.76 kJ mol^{-1} and 126.11 kJ mol^{-1}, respectively, for MWCNT when CR was replaced by PR.

The $\Delta_{ads}H^{\infty}$ parameter can be expressed as the sum of the same terms in Eq. (10), with the exception of the terms associated with the dye-dye interactions on the adsorbent surface ($\Delta_{ads}H^{D-D,Sur}$) and in the solution ($\Delta_{ads}H^{D-D,Sol}$), which are absent at infinite dilution. Thus, $\Delta_{ads}H^{\infty} = \Delta_{ads}H^{des,\infty} + \Delta_{ads}H^{D-S,\infty}$, with both $\Delta_{ads}H^{des,\infty}$ and $\Delta_{ads}H^{D-S,\infty}$ depending on the hydrophobicity and the charge density of the dye and the adsorbent. The $\Delta_{ads}H^{D-S,\infty}$ term became more negative as the electrostatic attraction between the dye and the adsorbent (which was positively charged at the pH evaluated) increased, i.e., as the negative charge density of the dye increased. Whereas the negative charge density increases in the order CR < AR < PR, $\Delta_{dds}H^{D-S,\infty}$(PR) < $\Delta_{ads}H^{D-S,\infty}$(AR) < $\Delta_{ads}H^{D-S,\infty}$(CR), which is in the same order of the $\Delta_{ads}H^{\infty}$ increase. On the other hand, the magnitude of the $\Delta_{ads}H^{des,\infty}$ term depends on the water-dye interaction intensity and on the number of water molecules released from the solvation shell of both adsorbent and dye when the dye adsorbs. Whereas CR has a larger ionic volume than PR and AR, it should interact with the adsorbent and release a greater number of water molecules to the bulk solution. Consequently, because of the highly hydrophobic nature of CR, the $\Delta_{ads}H^{des,\infty}$ term should be less negative (or more positive), contributing to the less negative values of $\Delta_{ads}H^{\infty}$ for this dye. The greater number of water molecules released to the bulk solution from the hydrophobic surfaces of both the adsorbent and CR also explains the less negative $T\Delta_{ads}S^{\infty}$ values for the CR adsorption.

Regarding the effect of the adsorbent structure on the adsorption

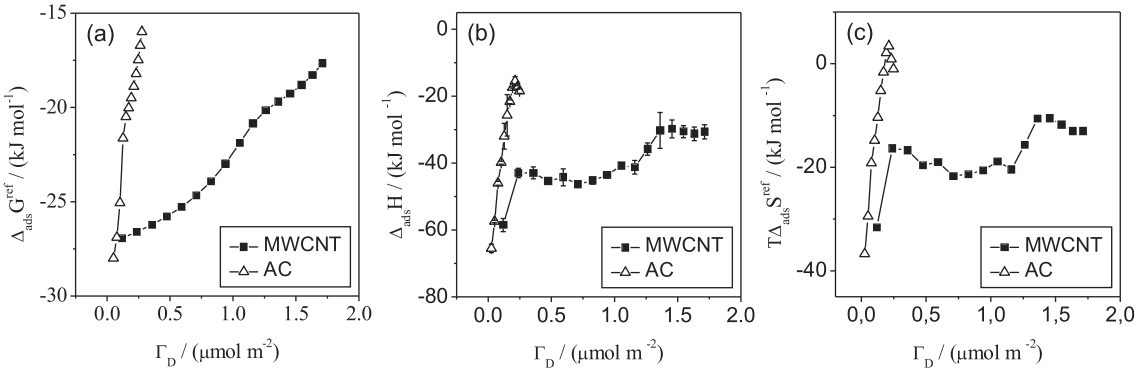

Fig. 7. Effect of adsorbent structure on (a) $\Delta_{ads}G^{ref}$, (b) $\Delta_{ads}H$, and (c) $T\Delta_{ads}S^{ref}$ for CR adsorption, at 25.0 °C and pH_i = 6.0.

thermodynamic parameters, the $\Delta_{ads}G^{\infty}$ values were slightly more negative for the AR and PR dyes when MWCNT was used as the adsorbent. Interestingly, the $\Delta_{ads}H^{\infty}$ values changed slightly when MWCNT was replaced by AC. Considering the deviation of the measurements, the differences between the $\Delta_{ads}H^{\infty}$ values obtained for MWCNT and AC, for each dye, were smaller than 2.0 kJ mol^{-1} (less than 3%). This indicated that the dyes interacted with similar sites on the surfaces of both adsorbents under infinite dilution conditions (i.e., sites with similar hydrophilicity). Consequently, the different adsorption capacities of AC and MWCNT were mainly due to the different interactions that occurred at higher Γ_D values.

4. Conclusions

The adsorption of red azo dyes on MWCNT and AC surfaces was utilized as molecular probes to highlight features of the adsorbent surfaces. Adsorption isotherms of the dyes depended on the structures of both the adsorbent and the dye. The driving force governing the adsorption of the dyes on both MWCNT and AC was the same, with the adsorption being enthalpically driven and associated with decreased entropy of the system.

At low surface coverage of both adsorbents the dye-adsorbent interactions occurred with a more negative enthalpy change, showing that electrostatic attractions, hydrogen bonds and ion-dipole interactions were involved in the adsorption process, besides π-π stacking. At the same time, the most hydrophilic sites on the surfaces were preferentially occupied and the enthalpic energy released due to the interaction between the hydrophilic sites and the dyes (at infinite dilution condition) did not depend on the adsorbent structure. The main factor responsible for determining the amounts of dye adsorbed on each adsorbent was electrostatic repulsion between the adsorbed dye molecules.

Acknowledgments

The authors are grateful for the financial support provided by Fundação de Amparo à Pesquisa do Estado de Minas Gerais (FAPEMIG), Conselho Nacional de Pesquisa e Desenvolvimento Tecnológico (CNPq), Instituto Nacional de Ciências e Tecnologias Analíticas Avançadas (INCTAA), and Financiadora de Estudos e Projetos (FINEP). G.M.D.F. and G.M.D.F. acknowledge research fellowships from Coordenação de Aperfeiçoamento de Pessoal de Nível Superior (CAPES).

Appendix A. Supplementary data

Figures showing ΔpH versus pH_icurves (Fig. S1); ITC dilution curves of red dyes in water (Fig. S2); adsorption enthalpy, entropy and Gibbs free energy changes versus Γ_D of red dyes (Figs. S3, S4 and S5); curves of integral adsorption enthalpy change versus Γ_D (Fig. S6). Supplementary data associated with this article can be found, in the online version, at http://dx.doi.org/10.1016/j.colsurfa.2017.06.021.

References

[1] K.-T. Chung, G.E. Fulk, A.W. Andrews, Mutagenicity testing of some commonly used dyes, Appl. Environ. Microbiol. 42 (1981) 641–648.
[2] K. Golka, S. Kopps, Z.W. Myslak, Carcinogenicity of azo colorants: Influence of solubility and bioavailability, Toxicol. Lett. 151 (2004) 203–210.
[3] E. Forgacs, T. Cserháti, G. Oros, Removal of synthetic dyes from wastewaters: a review, Environ. Int. 30 (2004) 953–971.
[4] V.K. Gupta, Suhas, Application of low-cost adsorbents for dye removal—a review, J. Environ. Manage. 90 (2009) 2313–2342.
[5] R.M.M. Santos, R.G.L. Gonçalves, V.R.L. Constantino, C.V. Santilli, P.D. Borges, J. Tronto, F.G. Pinto, Adsorption of Acid Yellow 42 dye on calcined layered double hydroxide: Effect of time, concentration, pH and temperature, Appl. Clay Sci. 140 (2017) 132–139.
[6] G. Orlandi, J. Cavasotto, F.R.S. Machado Jr., G.L. Colpani, J.D. Magro, F. Dalcanton, J.M.M. Mello, M.A. Fiori, An adsorbent with a high adsorption capacity obtained from the cellulose sludge of industrial residues, Chemosphere 169 (2017) 171–180.
[7] B. Satilmis, P.M. Budd, Selective dye adsorption by chemically-modified and thermally-treated polymers of intrinsic microporosity, J. Colloid Interface Sci. 492 (2017) 81–91.
[8] V.K. Gupta, R. Kumar, A. Nayak, T.A. Saleh, M.A. Barakat, Adsorptive removal of dyes from aqueous solution onto carbon nanotubes: a review, Adv. Colloid Interface Sci. 193–194 (2013) 24–34.
[9] P. Sharma, B.K. Saikia, M.R. Das, Removal of methyl green dye molecule from aqueous system using reduced graphene oxide as an efficient adsorbent: Kinetics, isotherm and thermodynamic parameters, Colloids Surf A 457 (2014) 125–133.
[10] H.S. Saroyan, D.A. Giannakoudakis, C.S. Sarafidis, N.K. Lazaridis, E.A. Deliyanni, Effective impregnation for the preparation of magnetic mesoporous carbon: Application to dye adsorption, J. Chem. Technol. Biotechnol. (2017), http://dx.doi.org/10.1002/jctb.5210.
[11] H.N. Tran, S.J. You, H.P. Chao, Fast and efficient adsorption of methylene green 5 on activated carbon prepared from new chemical activation method, J. Environ. Manage. 188 (2017) 322–336.
[12] M.A. Islam, M.J. Ahmed, W.A. Khanday, M. Asif, B.H. Hameed, Mesoporous activated carbon prepared from NaOH activation of rattan (*Lacosperma secundiflorum*) hydrochar for methylene blue removal, Ecotoxicol. Environ. Saf. 138 (2017) 279–285.
[13] M. Yu, J. Li, L. Wang, KOH-activated carbon aerogels derived from sodium carboxymethyl cellulose for high-performance supercapacitors and dye adsorption, Chem. Eng. J. 310 (2017) 300–306.
[14] F. Marrakchi, M.J. Ahmed, W.A. Khanday, M. Asif, B.H. Hameed, Mesoporous-activated carbon prepared from chitosan flakes via single-step sodium hydroxide activation for the adsorption of methylene blue, Int. J. Biol. Macromol. 98 (2017) 233–239.
[15] H. Saygılı, F. Güzel, Y. Önal, Conversion of grape industrial processing waste to activated carbon sorbent and its performance in cationic and anionic dyes adsorption, J. Clean. Prod. 93 (2015) 84–93.
[16] C. Yu, J.S. Qiu, Y.F. Sun, X.H. Li, G. Chen, Z.B. Zhao, Adsorption removal of thiophene and dibenzothiophene from oils with activated carbon as adsorbent: Effect of surface chemistry, J. Porous Mater. 15 (2007) 151–157.
[17] K. Yang, B.S. Xing, Adsorption of organic compounds by carbon nanomaterials in aqueous phase: Polanyi theory and its application, Chem. Rev. 110 (2010) 5989–6008.
[18] S. Mashhadi, H. Javadian, M. Ghasemi, T.A. Saleh, V.K. Gupta, Microwave-induced H_2SO_4 activation of activated carbon derived from rice agricultural wastes for sorption of methylene blue from aqueous solution, Desalin. Water Treat. 57 (2016) 21091–21104.
[19] B.H. Hameed, A.T.M. Din, A.L. Ahmad, Adsorption of methylene blue onto bamboo-based activated carbon: kinetics and equilibrium studies, J. Hazard. Mater. 141 (2007) 819–825.
[20] C.H. Wu, Adsorption of reactive dye onto carbon nanotubes: Equilibrium, kinetics and thermodynamics, J. Hazard. Mater. 144 (2007) 93–100.
[21] Y.J. Yao, F.F. Xu, M. Chen, Z.X. Xu, Z.W. Zhu, Adsorption behavior of methylene blue on carbon nanotubes, Bioresour. Technol. 101 (2010) 3040–3046.
[22] C.Y. Kuo, C.H. Wu, J.Y. Wu, Adsorption of direct dyes from aqueous solutions by carbon nanotubes: Determination of equilibrium, kinetics and thermodynamics parameters, J. Colloid Interface Sci. 327 (2008) 308–315.
[23] F.M. Machado, S.A. Carmalin, E.C. Lima, S.L.P. Dias, L.D.T. Prola, C. Saucier, I.M. Jauris, I. Zanella, S.B. Fagan, Adsorption of Alizarin Red S dye by carbon nanotubes: An experimental and theoretical investigation, J. Phys. Chem. C 120 (2016) 18296–18306.
[24] A. Peigney, C. Laurent, E. Flahaut, R.R. Bacsa, A. Rousset, Specific surface area of carbon nanotubes and bundles of carbon nanotubes, Carbon 39 (2001) 507–514.
[25] F.M. Machado, C.P. Bergmann, E.C. Lima, B. Royer, F.E. de Souza, I.M., Jauris, T., Calvete, S.B., Fagan, Adsorption of reactive blue 4 dye from water solutions by carbon nanotubes: experiment and theory, Phys. Chem. Chem. Phys. 14 (2012) 11139–11153.
[26] C.H. Liu, J.J. Li, H.L. Zhang, B.R. Li, Y. Guo, Structure dependent interaction between organic dyes and carbon nanotubes, Colloids Surf. A 313 (2008) 9–12.
[27] Y.H. Li, Q.J. Du, T.H. Liu, X.J. Peng, J.J. Wang, J.K. Sun, Y.H. Wang, S.L. Wu, Z.H. Wang, Y.Z. Xia, L.H. Xia, Comparative study of methylene blue dye adsorption onto activated carbon, graphene oxide, and carbon nanotubes, Chem. Eng. Res. Des. 91 (2013) 361–368.
[28] A. Ahmad, M.H. Razali, M. Mamat, F.S.B. Mehamod, K. Anuar Mat Amin, Adsorption of methyl orange by synthesized and functionalized-CNTs with 3-aminopropyltriethoxysilane loaded TiO_2 nanocomposites, Chemosphere 168 (2017) 474–482.
[29] A. Maleki, U. Hamesadeghi, H. Daraei, B. Hayati, F. Najafi, G. McKay, R. Rezaee, Amine functionalized multi-walled carbon nanotubes: single and binary systems for high capacity dye removal, Chem. Eng. J. 313 (2017) 826–835.
[30] S. Qu, F. Huang, S. Yu, G. Chen, J. Kong, Magnetic removal of dyes from aqueous solution using multi-walled carbon nanotubes filled with Fe_2O_3 particles, J. Hazard. Mater. 160 (2008) 643–647.
[31] J.L. Gong, B. Wang, G.M. Zeng, C.P. Yang, C.G. Niu, Q.Y. Niu, W.J. Zhou, Y. Liang, Removal of cationic dyes from aqueous solution using magnetic multi-wall carbon nanotube nanocomposite as adsorbent, J. Hazard. Mater. 164 (2009) 1517–1522.
[32] S. Saber-Samandari, S. Saber-Samandari, H. Joneidi-Yekta, M. Mohseni, Adsorption of anionic and cationic dyes from aqueous solution using gelatin-based magnetic nanocomposite beads comprising carboxylic acid functionalized carbon nanotube, Chem. Eng. J. 308 (2017) 1133–1144.
[33] L.D. Prola, F.M. Machado, C.P. Bergmann, F.E. de Souza, C.R. Gally, E.C. Lima, M.A. Adebayo, S.L. Dias, T. Calvete, Adsorption of Direct Blue 53 dye from aqueous solutions by multi-walled carbon nanotubes and activated carbon, J. Environ.

Manage. 130 (2013) 166–175.
[34] F.M. Machado, C.P. Bergmann, T.H.M. Fernandes, E.C. Lima, B. Royer, T. Calvete, S.B. Fagan, Adsorption of reactive red M-2BE dye from water solutions by multi-walled carbon nanotubes and activated carbon, J. Hazard. Mater. 192 (2011) 1122–1131.
[35] M. Farré, J. Sanchís, D. Barceló, Adsorption and desorption properties of carbon nanomaterials, the potential for water treatments and associated risks, in: G. Lofrano, G. Libralato, J. Brown (Eds.), Nanotechnologies for Environmental Remediation: Applications and Implications, Springer International Publishing, Cham, 2017, pp. 137–182.
[36] S.J. Sarma, I. Bhattacharya, S.K. Brar, R.D. Tyagi, R.Y. Surampalli, Carbon nanotube—bioaccumulation and recent advances in environmental monitoring, Crit. Rev. Env. Sci. Technol. 45 (2015) 905–938.
[37] H.N. Tran, Y.-F. Wang, S.-J. You, H.-P. Chao, Insights into the mechanism of cationic dye adsorption on activated charcoal: the importance of π–π interactions, Process. Saf. Environ. Prot. 107 (2017) 168–180.
[38] T. Blaschke, A. Werner, H. Hasse, Microcalorimetric study of the adsorption of native and mono-PEGylated bovine serum albumin on anion-exchangers, J. Chromatogr. A 1277 (2013) 58–68.
[39] W.Y. Chen, H.M. Huang, C.C. Lin, F.Y. Lin, Y.C. Chan, Effect of temperature on hydrophobic interaction between proteins and hydrophobic adsorbents: Studies by isothermal titration calorimetry and the van't Hoff equation, Langmuir 19 (2003) 9395–9403.
[40] Z. Wang, S. Xu, E. Acosta, Heat of adsorption of surfactants and its role on nanoparticle stabilization, J. Chem. Thermodyn. 91 (2015) 256–266.
[41] X. Wang, K. Zhao, B. Yang, T. Chen, D. Li, H. Wu, J. Wei, X. Wu, Adsorption of dibutyl phthalate in aqueous solution by mesoporous calcium silicate grafted nonwoven polypropylene, Chem. Eng. J. 306 (2016) 452–459.
[42] L. Fang, P. Cai, P. Li, H. Wu, W. Liang, X. Rong, W. Chen, Q. Huang, Microcalorimetric and potentiometric titration studies on the adsorption of copper by *P. putida* and *B. thuringiensis* and their composites with minerals, J. Hazard. Mater. 181 (2010) 1031–1038.
[43] D.L. Guerra, A.C. Batista, R.R. Viana, C. Airoldi, Adsorption of methylene blue on raw and MTZ/imogolite hybrid surfaces: effect of concentration and calorimetric investigation, J. Hazard. Mater. 183 (2010) 81–86.
[44] P.F.R. Ortega, J.P.C. Trigueiro, M.R. Santos, A.M.L. Denadai, L.C.A. Oliveira, A.P.C. Teixeira, G.G. Silva, R.L. Lavall, Thermodynamic study of methylene blue adsorption on carbon nanotubes using isothermal titration calorimetry: a simple and rigorous approach, J. Chem. Eng. Data 62 (2017) 729–737.
[45] S. Brunauer, P.H. Emmett, E. Teller, Adsorption of gases in multimolecular layers, J. Am. Chem. Soc. 60 (1938) 309–319.
[46] L.H. Ai, C.Y. Zhang, F. Liao, Y. Wang, M. Li, L.Y. Meng, J. Jiang, Removal of methylene blue from aqueous solution with magnetite loaded multi-wall carbon nanotube: kinetic, isotherm and mechanism analysis, J. Hazard. Mater. 198 (2011) 282–290.
[47] T. Blaschke, J. Varon, A. Werner, H. Hasse, Microcalorimetric study of the adsorption of PEGylated lysozyme on a strong cation exchange resin, J. Chromatogr. A 1218 (2011) 4720–4726.
[48] B. Prelot, I. Ayed, F. Marchandeau, J. Zajac, On the real performance of cation exchange resins in wastewater treatment under conditions of cation competition: the case of heavy metal pollution, Environ. Sci. Pollut. Res. Int. 21 (2014) 9334–9343.
[49] M. Kragulj, J. Tričković, B. Dalmacija, Á. Kukovecz, Z. Kónya J. Molnar, S. Rončević, Molecular interactions between organic compounds and functionally modified multiwalled carbon nanotubes, Chem. Eng. J. 225 (2013) 144–152.
[50] M.R. Almeida, R. Stephani, H.F.D. Santos, L.F.C.D. Oliveira, Spectroscopic and theoretical study of the azo-dye E124 in condensate chase: evidence of a dominant hydrazo form, J. Phys. Chem. A 114 (2010) 526–534.
[51] A.J. Brooks, H.N. Lim, J.E. Kilduff, Adsorption uptake of synthetic organic chemicals by carbon nanotubes and activated carbons, Nanotechnology 23 (2012) 294008.
[52] V.K.K. Upadhyayula, S.G. Deng, M.C. Mitchell, G.B. Smith, Application of carbon nanotube technology for removal of contaminants in drinking water: a review, Sci. Total Environ. 408 (2009) 1–13.
[53] N. Mourtzis, G. Cordoyiannis, G. Nounesis, K. Yannakopoulou, Single and double threading of congo red into γ-cyclodextrin. Solution structures and thermodynamic parameters of 1:1 and 2:2 adducts, as obtained from NMR spectroscopy and microcalorimetry, Supramol. Chem. 15 (2003) 639–649.
[54] M. Skowronek, B. Stopa, L. Konieczny, J. Rybarska, B. Piekarska, E. Szneler, G. Bakalarski, I. Roterman, Self-assembly of Congo Red—a theoretical and experimental approach to identify its supramolecular organization in water and salt solutions, Biopolymers 46 (1998) 267–281.